www.entechnol.de

Photothermal Utility Heating with Diffused Indoor Light via Multiple Transparent $Fe_3O_4@Cu_{2-x}S$ Thin Films

Anudeep Katepalli, Neshwanth Kumar Tene, Yuxin Wang, Anton Harfmann, Mathias Bonmarin, John Krupczak, and Donglu Shi*

By introducing a novel photothermal radiator that effectively harnesses diffused light through plasmonic Fe₃O₄@Cu_{2-x}S nanoparticles, it is sought to offer a sustainable solution for maintaining comfortable indoor temperatures without heavy reliance on traditional solar sources. The approach involves the use of ultraviolet (UV) and infrared (IR) lights to photothermally activate transparent Fe₃O₄@Cu_{2-x}S thin films, showcasing a proactive strategy to optimize energy capture even in low-light scenarios such as cloudy days or nighttime hours. This innovative technology carries immense potential for energy-neutral buildings, paving the way to reduce dependence on external energy grids and promoting a more sustainable future for indoor heating and comfort control. The developed photothermal radiator incorporates multiple transparent thin films infused with plasmonic Fe₃O₄@Cu_{2-x}S nanoparticles, known for their robust UV and IR absorptions driven by localized surface plasmon resonance. Through the application of UV and IR lights, these thin films efficiently convert incident photons into thermal energy. The experiments within a specially constructed diffused light photothermal box, designed to simulate indoor environments, demonstrate the system's capability to raise temperatures above 50 °C effectively. This pioneering photothermal radiator offers a promising pathway for sustainable heat generation in indoor spaces, harnessing ubiquitous diffused light sources to enhance energy efficiency.

A. Katepalli, N. K. Tene, Y. Wang, D. Shi Materials Science and Engineering Program Department of Mechanical and Materials Engineering College of Engineering and Applied Science University of Cincinnati Cincinnati, OH 45221, USA E-mail: shid@ucmail.uc.edu

A. Harfmann College of Design, Architecture, Art and Planning University of Cincinnati Cincinnati, OH 45221, USA

M. Bonmarin School of Engineering Zurich University of Applied Sciences 8400 Winterthur, Switzerland

J. Krupczak Department of Engineering Hope College Holland, MI 49423, USA

The ORCID identification number(s) for the author(s) of this article can be found under https://doi.org/10.1002/ente.202400703.

DOI: 10.1002/ente.202400703

1. Introduction

Transitioning toward energy-neutral structures presents a multitude of advantages, ranging from reduced utility costs to bolstered grid reliability, improved air quality, public health benefits, and the creation of a carbon-free environment.[1] Amidst these pressing energy challenges, photothermal (PT) energy emerges as a beacon of promise, offering a plethora of technical, environmental, and ecological advantages. [2,3] The widespread adoption of photovoltaic (PV) solar cells has undeniably marked a significant stride toward sustainable energy generation. However, as commendable as their deployment has been, the limitations inherent in traditional PV systems have spurred a quest for innovative and more efficient alternatives. [3-10] One prominent limitation is the reliance of PV solar cells on direct sunlight, rendering them inactive during inclement weather and nighttime hours. This inherent intermittency in energy generation poses challenges to achieving round-the-clock renewable energy availability. Furthermore, the con-

ventional focus of solar energy research has predominantly centered on harnessing sunlight as the primary photon source. Yet, a vast untapped potential lies in exploring the generation of energy from alternative photon sources, particularly diffused lights that persist in buildings during nighttime hours. The investigation into novel methods for energy generation under low-light conditions not only promises to enhance the efficiency and reliability of solar energy systems but also opens avenues for sustainable energy production throughout various environmental conditions.

In modern urban landscapes, the energy efficiency of public buildings and high rises stands as a critical concern, particularly as these structures often require illumination throughout the night for security purposes, such as guiding emergency responders and enhancing building safety. The utilization of diffused light for PT heating via plasmonic nanoparticles presents a promising avenue for energy-efficient applications. [11–13] While the PT effects of plasmonic nanoparticles have been well established under direct solar illumination, the potential of harnessing diffused light remains largely unexplored. Unlike direct sunlight, diffused light within indoor environments or shaded areas lacks

the intense, focused irradiance typically associated with conventional solar exposure. However, this very characteristic of diffused light offers a unique opportunity for PT applications. The scattering and multiple reflections of light within a confined space, such as a building interior, create a more uniform and distributed light field. Plasmonic nanoparticles, such as Fe₃O₄@Cu_{2-x}S, with their inherent ability to efficiently convert light into heat through the localized surface plasmon resonance (LSPR) effect, can be strategically employed in such environments. $^{[15-17]}$

By introducing these plasmonic nanoparticles into transparent thin films or coatings, the diffused light present within buildings can be effectively harvested for PT heating purposes. The nanoparticles, dispersed within the transparent matrix, can spectral selectively absorb a broad range of wavelengths, including those within the UV and infrared (IR) spectra. This allows for the absorption of light energy from the diffused sources, initiating the PT conversion process. This innovative approach not only offers a means to reduce reliance on traditional heating systems but also contributes to the overall energy efficiency of buildings. Furthermore, the utilization of diffused light for PT heating aligns with the broader goal of sustainable and environmentally friendly building practices. As such, exploring the potential of plasmonic nanoparticles in capturing and converting diffused light into thermal energy represents a promising frontier in the realm of energy-efficient building technologies.

The PT effect attributed to LSPR is a captivating phenomenon rooted in the confinement of surface plasmons within nanoparticles of sizes comparable to or smaller than the wavelength of incident light. [18–28] Upon exposure to light, especially in the case of nanoparticles, the oscillating electric field of the light instigates a collective oscillation of conduction electrons within the nanoparticle, resonating in coherence. This collective oscillation induces a restoring force arising from the Coulombic attraction between the electrons and the nanoparticle's nuclei, thereby sustaining the electron cloud's oscillation. The frequency of this oscillation is determined by a complex interplay of factors including electron density, effective electron mass, and the size as well as the morphology of the nanoparticle's charge distribution. [15–18]

The PT effect exhibited by $Fe_3O_4@Cu_{2-x}S$ nanoparticles is intricately tied to the phenomenon of LSPR, offering a fascinating avenue for efficient light-to-heat conversion. The tunability of the LSPR frequency in $Fe_3O_4@Cu_{2-x}S$

nanoparticles offers a versatile platform for optimizing the PT response.[19-21,23-27,29-31] Although the noble metal nanoparticles exhibit strong PT effects, their resonances typically emerge within the visible wavelength spectrum, [29] rendering them nontransparent. Fe₃O₄@Cu_{2-x}S nanoparticles are composed of a core-shell structure with Fe_3O_4 at the core and $Cu_{2-x}S$ as the shell, resulting in unique optical properties.^[30,31] As shown in Figure 1a, the Fe₃O₄ and Fe₃O₄@Cu_{2-x}S nanoparticles are characterized with distinctive optical behaviors, while the former exhibits only the UV absorption, the latter displays strong and broad peak in the IR region. This characteristic "U"-shaped absorption spectrum results from the core-shell structure, which is responsible for the broad IR absorption. [18–21,23–27] Crucially, this optical feature showcases a minimum within the visible spectrum, making it particularly advantageous for the fabrication of transparent thin films. The presence of this minimum in the visible band allows for the efficient transmission of visible light through multiple PT panels (Figure 1b) for collective heat generation.

As shown in Figure 1b, by employing multiple layers of transparent films coated with $Fe_3O_4@Cu_{2-x}S$ nanoparticles, each panel is capable of harvesting light across a broad spectrum. This collective light harvesting capability enables the entire array of panels to function collectively as a PT radiator. As each layer of the thin film absorbs photons from the incident light, the accumulated energy is photothermally converted into heat via the LSPR effect. This innovative approach holds tremendous potential for efficiently harnessing diffused light within buildings, offering a sustainable solution for building heating utilities.

The primary objective of this research is to determine if diffused light sources within buildings could generate sufficient heat to compensate for building utility heating, as illustrated in Figure 2. Building upon the fundamental principles elucidated in Figure 1, the core objective of this experimental endeavor is to deliberately activate the PT effect within the PT radiator utilizing diffused light sources. This activation is aimed at inducing heat generation, through multiple transparent photothermal panels (TPTPs). The overarching aim of this research is to ascertain the potential of generating adequate thermal energy from diffused lights to sustain a comfortable room temperature, particularly in cold climate conditions, during nighttime, and under cloudy or rainy weather scenarios. Furthermore, understanding the efficiency of diffused light for PT heating can pave the way for

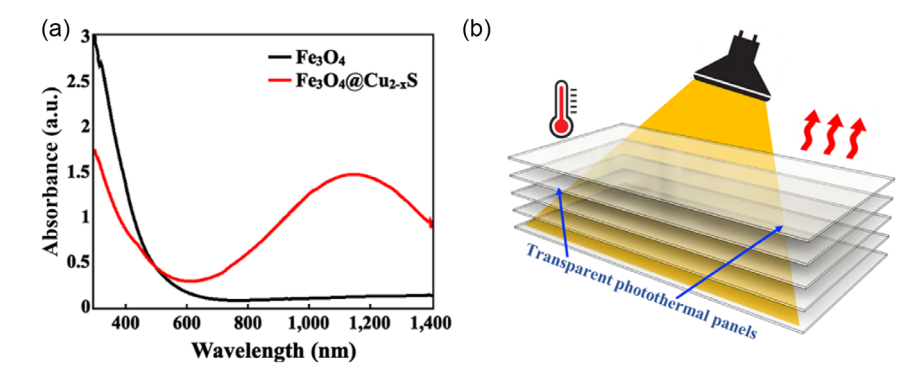


Figure 1. a) Absorption spectra of the Fe_3O_4 and Fe_3O_4 @ $Cu_{2-x}S$ nanoparticles dispersed in toluene (0.1 mg mL $^{-1}$) and b) schematic PT heating via diffused light with multiple transparent plasmonic thin films. $^{[23-27]}$

Photothermal radiator

Photothermal radiator

Photothermal radiator

Photothermal radiator

Figure 2. A schematic diagram showing the concept of the PT radiator with multiple transparent PT panels via diffused lights within the buildings.

tailored strategies to optimize energy utilization in public buildings and high rises. A key aspect of this study involves identifying the most efficient frequency of the light source for the PT effect of the plasmonic materials. This aspect of the research is essential for maximizing the energy conversion efficiency and ensuring optimal utilization of available light sources. By developing the relationship between different light frequencies and the absorptions of the plasmonic particles, we aim to pinpoint the ideal conditions for achieving efficient PT heating.

2. Experimental Section

2.1. Synthesis of $Fe_3O_4@Cu_{2-x}S$ Nanoparticles and Deposition of Thin Films

The synthesis of Fe_3O_4 nanoparticles commenced with the heating of a 60 mL oleylamine solution to 300 °C within a nitrogen environment, accompanied by the injection of $Fe(acac)_3$ in oleylamine/N-methyl-2-pyrrolidone. ^[23,27,28] Upon thorough mixing at 300 °C, the solution underwent cooling to 60 °C, after which the Fe_3O_4 nanoparticles were gathered, cleansed with methanol, and subsequently dried through freeze drying techniques.

Subsequently, the Fe $_3O_4$ nanoparticles were coated with Cu $_{2-x}S$. This process involved the heating of a specified volume of the Fe $_3O_4$ nanoparticle solution to 70 °C. A mixture of sulfur in oleylamine/cyclohexane was then introduced into the solution, followed by the addition of Cu(acac) $_2$ in oleylamine/chloroform. Afterward, the resulting Fe $_3O_4$ @Cu $_{2-x}S$ nanoparticles were collected, subjected to thorough washing, and dried to yield the final product. For the deposition of thin films, a 10 mL solution of Fe $_3O_4$ @Cu $_{2-x}S$ nanoparticles was mixed with 80 mL of epoxy resin. [23,27,28] The polymer solution was stirred for 5 min to ensure uniform mixing and the removal of any trapped air bubbles. Subsequently, 10 mL of this well-mixed solution was evenly distributed onto each of eight glass panels, resulting in a concentration of Fe $_3O_4$ @Cu $_{2-x}S$ nanoparticles of 0.006 mg cm $^{-2}$ on

each panel, achieving 75% AVT. After distribution, the panels were allowed to cure overnight, ensuring that the polymer solution fully cured, and the thin films were ready for use in subsequent applications.

2.2. Experimental Setup

To simulate indoor conditions and investigate the heating effectiveness under diffused light, a diffused light photothermal box (DLPB) was custom-built (Figure 3).[32] The TPTPs used in the experiment were coated with the Fe₃O₄@Cu_{2-x}S thin films. The design of the DLPB was tailored to mimic building environments, featuring a vertical PT tunnel encased within a transparent polymethyl methacrylate (PMMA) box measuring 50 cm (length) \times 37 cm (width) \times 50 cm (height). Within this PT tunnel, eight removable TPTPs were arranged horizontally in parallel for efficient photon collection (Figure 3a). To enhance energy harvesting, the interior of the tunnel was lined with mirrors to effectively reflect photons. Each TPTP utilized in the experiment was crafted with dimensions of 18 cm (length) × 13 cm (width) × 3 mm (height), ensuring a uniform heating surface area throughout the study. Figure 3b depicts an actual photograph of the constructed DLPB, with its internal PT tunnel utilized for conducting the PT experiments in this investigation.

The average visible transmittance (AVT) of the PT panels was precisely maintained at 75%, while that of the polymethyl methacrylate (PMMA) box enclosing the setup was maintained at 93%. As shown in Figure 3c, both IR and UV lamps are utilized to simulate diffused lights. The IR and UV lamps emit light with the wavelengths of 660–850 nm and 380–420 nm, respectively. The light power density (LPD) for all lighting conditions is controlled at 15 mW cm⁻². LPD measurements are obtained using the Newport Optical Power Meter Model 1600-R.

The transparent PT panels are exposed to three different lighting conditions: 1) 3 IR lamps (the power of each IR lamp: 56 W), 2) 3 UV lamps (the power of each UV lamp: 100 W), and

www.advancedsciencenews.com www.entechnol.de

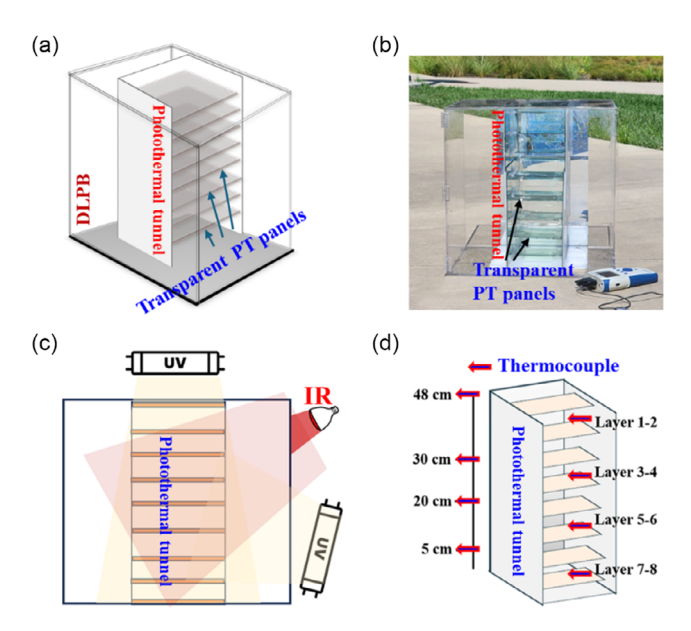


Figure 3. a) Schematic diagram showing DLPB, b) photograph of DLPB, c) schematic diagram showing the IR and UV lamps outside the DLPB, and d) schematic diagram showing the PT tunnel with the locations of the thermocouples. Note that the thermocouples are placed within and outside the PT tunnel inside the DLPB at the different heights as indicated.

3) 3 IR + 3 UV lamps. For conditions (1) and (2), the lamps are placed 30 cm away from the front side of the PT panels to enhance LPD. For condition (3), the lamps are placed 20 cm away from the front side and 5 cm away from the top of the PT panels. Figure 3d is the schematic of DLPB with the transparent PT panels arranged in parallel. K-type thermocouples are utilized to monitor temperatures between the TPTPs and within the DLPB at different heights (e.g., 5, 20, 30, and 40 cm). Upon turning the UV and IR lights on, the temperatures at these locations are measured and plotted in the temperature versus time heating curves.

3. Results

3.1. Characterization of the Fe $_3O_4$ @Cu $_{2-x}S$ Nanoparticles and Thin Films

The synthesis and characterization of Fe₃O₄ and Fe₃O₄@Cu_{2-x}S nanoparticles, along with their thin films, have been previously documented in literature. [18-28] **Figure 4**a,b presents transmission electron microscopy (TEM) images of the Fe₃O₄ and Fe₃O₄@Cu_{2-x}S nanoparticles, respectively. These images reveal their monodispersed nature, with an average diameter of 10 nm for the former and 15 nm for the latter due to the presence of the Cu_{2-x}S shell on the Fe₃O₄ nanoparticle. Upon the application of the nanoparticle solution onto glass substrates through spin coating, uniform thin films were successfully formed. [19,23,27,28] As shown in Figure 4c, the temperature increase, ΔT , over time for the Fe₃O₄@Cu_{2-x}S thin films at various concentrations under simulated solar light with a power of 0.1 W cm⁻² is displayed. The initial rapid rise in temperature is attributed to the PT effect of the thin films, eventually reaching a plateau after

 $\approx \! 5$ min. This plateau signifies an equilibrium between heat generation from PT film and heat dissipation to the surroundings. Subsequently, at the 25 minute mark, the light source is deactivated, resulting in a swift decline in temperature across all concentrations. Figure 4c delineates the heating curves corresponding to different film concentrations, with the highest temperature observed at 43.6 °C for a Fe₃O₄@Cu_{2-x}S concentration of $4.92\times 10^{-5}\,\mathrm{g\,cm^{-2}}$.

As shown in Figure 1a, the $Fe_3O_4@Cu_{2-x}S$ thin film displays a distinctive minimum in the visible region and broad absorption extending into the IR range, peaking at 1200 nm. [19,23,27,28] This unique optical feature provides the film with strong absorptions in the UV and near-IR (NIR) regions for efficient thermal energy conversion, alongside high transmittance in the visible range essential for multipanel applications. For comparative analysis, the optical absorption of the Fe₃O₄ thin film is also presented in Figure 1a. This film exhibits robust UV absorption; however, no peak is observed in the IR region. The distinctive "U"-shaped characteristic absorption spectrum depicted in Figure 1a is attributed to the addition of Cu_{2-x}S in the Fe₃O₄ system, creating a typical core-shell structure that accounts for the broad and significant IR absorption. [30] Previous studies have highlighted that the strong IR absorption of the $Fe_3O_4@Cu_{2-x}S$ film significantly enhances its PT effect. [19,23,27,28] Expanding on the optical properties, the Fe₃O₄@Cu_{2-x}S film displays remarkable transparency, as depicted in Figure 4d. This photograph captures a $Fe_3O_4@Cu_{2-x}S$ film with AVT of 75% positioned in front of a building on the University of Cincinnati campus. Figure 4e shows the absorbance of the Fe₃O₄ @Cu_{2-x} Sfilm displaying the "U"-shaped characteristic. This data is also consistent with the absorption of the Fe₃O₄ @Cu_{2-x} S nanoparticles dispersed in toluene (Figure 1a). The transmittance dataare shown in Figure 4. As can be seen in this figure, the transmittance in the visible region can reach 75% indicating high transparency. Multiple TPTPs, like the one shown in Figure 4d, are inserted into the DLPB for solar harvesting and thermal energy generation. Corresponding to the "U"-shaped optical characteristic illustrated in Figure 1a, the film exhibits high transparency, resulting in a clear image of the building at a distance. This high light transmittance in the "optical window" is a fundamental requirement for TPTPs, facilitating diffused light harvesting through multiple panels for enhanced energy efficiency.

3.2. PT Experiments

The PT experiments using the DLPB with all the conditions are detailed in Figure 3. Figure 5a is a photograph of the DLPB with only three IR lights placed in the front as indicated. Figure 5b,c shows the heating curves between the TPTP and within DLPB, respectively. The locations of the thermocouples are indicated in Figure 3d. As shown in these figures, the temperatures of all eight TPTPs experience rapid increase initially, and level off forming plateaus until the lights are turned off at 400 min. The temperature between the first and second layers reaches 37.3 °C after 100 min, indicating significant PT heating by the IR lights. Accordingly, the heating curves exhibit similar behaviors in the DLPB at different heights, reaching the highest temperature up to 29.2 °C at 20 cm.

www.advancedsciencenews.com www.entechnol.de

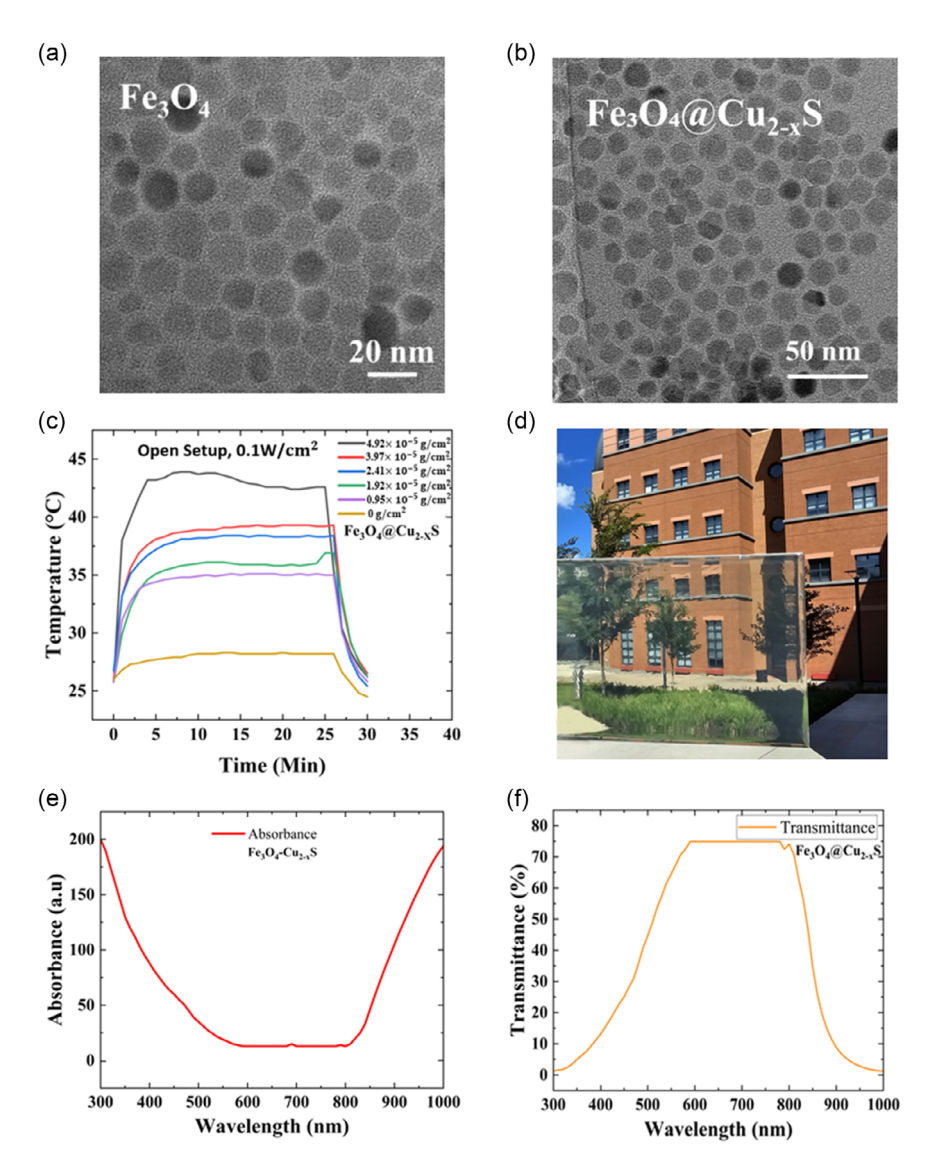


Figure 4. TEM images of a) Fe_3O_4 and b) Fe_3O_4 @Cu_{2-x}S nanoparticles; c) heating curves of Fe_3O_4 @Cu_{2-x}S thin films under simulated solar light with different nanoparticle concentrations indicated; d) photograph of the Fe₃O₄@Cu_{2-x}S thin film showing high transparency; e) absorbance; and f) transmittance of the $Fe_3O_4@Cu_{2-x}S$ thin film.

The calculation of thermal energy follows the formula $Q = \Delta T_{\text{max}} \times \text{m} \times C_{\text{p}}$, where ΔT represents the maximum temperature difference produced by a given number of thin films, m stands for the mass of the sample (including the thin film and substrate), and C_p denotes the specific heat of the glass panel (notably, the PT films are exceedingly thin). This thermal energy computation is derived from the heating curves of the Fe₃O₄@Cu_{2-x}S films installed in the DLPB and is graphically depicted against the number of layers in Figure 5d. The figure illustrates a notable escalation in thermal energy generation with the addition of more TPTP. Notably, the thermal energy calculation solely focuses on the heating curve, excluding the cooling curve, as its aim is to illustrate the maximum thermal energy generation across various layer stacks. As delineated in Figure 5d, the thermal energy produced aligns consistently with the heating curves presented in Figure 5b. For two panels within the DLPB, the system yields $\approx 1.0 \times 10^5$ J of thermal energy. With the inclusion of more panels, the generated thermal energy continues to rise steadily, reaching 4.3×10^5 J for a total of eight panels.

The optical photograph of the DLPB is depicted in Figure 6a, showing the arrangement with three UV lights: two positioned at the front and one at the top, as indicated. In Figure 6b, the heating curves obtained from various locations of the TPTPs are presented, with temperatures measured corresponding to the locations depicted in Figure 3d. The data displayed in this figure reveal a rapid increase in temperatures across all eight TPTPs in the first 100 min, reaching their respective maximum before the cessation of light. In contrast to the patterns observed under IR light alone, the maximum temperatures are significantly higher, reaching 48.1 °C between the first two layers. Similar trends are noted in the heating curves obtained at different heights within the DLPB, as shown in Figure 3d.

www.entechnol.de www.advancedsciencenews.com

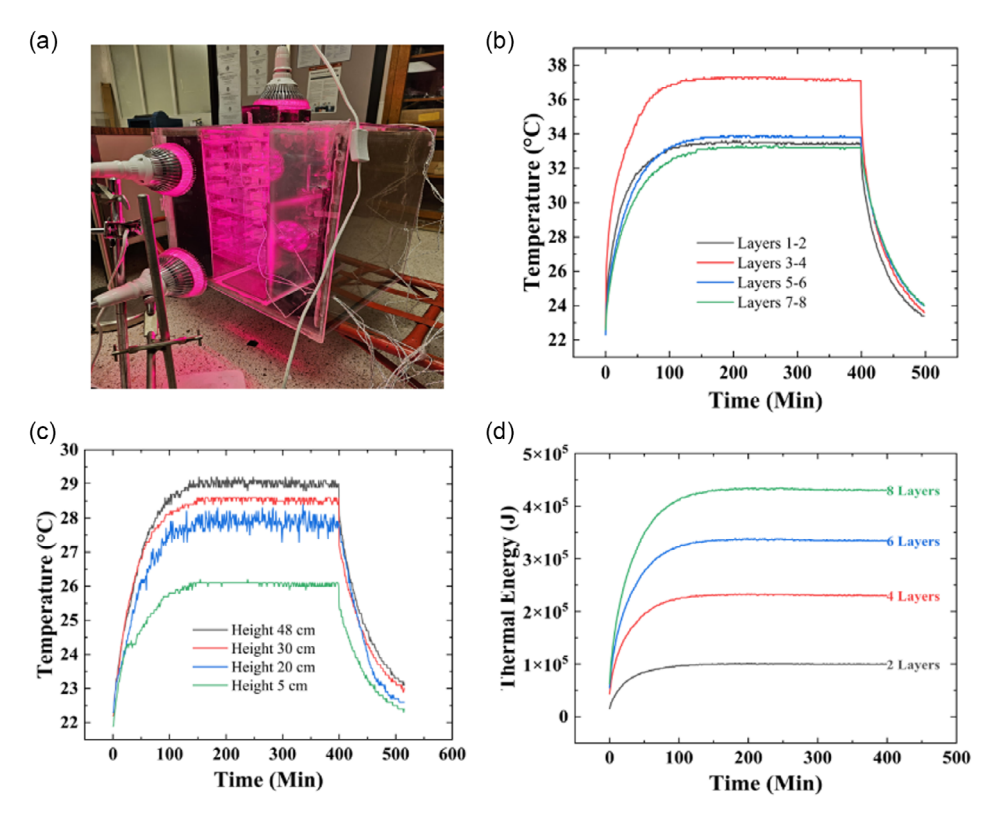


Figure 5. a) Schematic diagram showing the DLPB under three IR lights only; b) heating curves taken between different TPTPs; c) heating curves taken at different heights within the DLPB, and d) thermal energy versus number of panels. Ambient temperature: 21 °C. Light power density is 15 mW cm⁻².

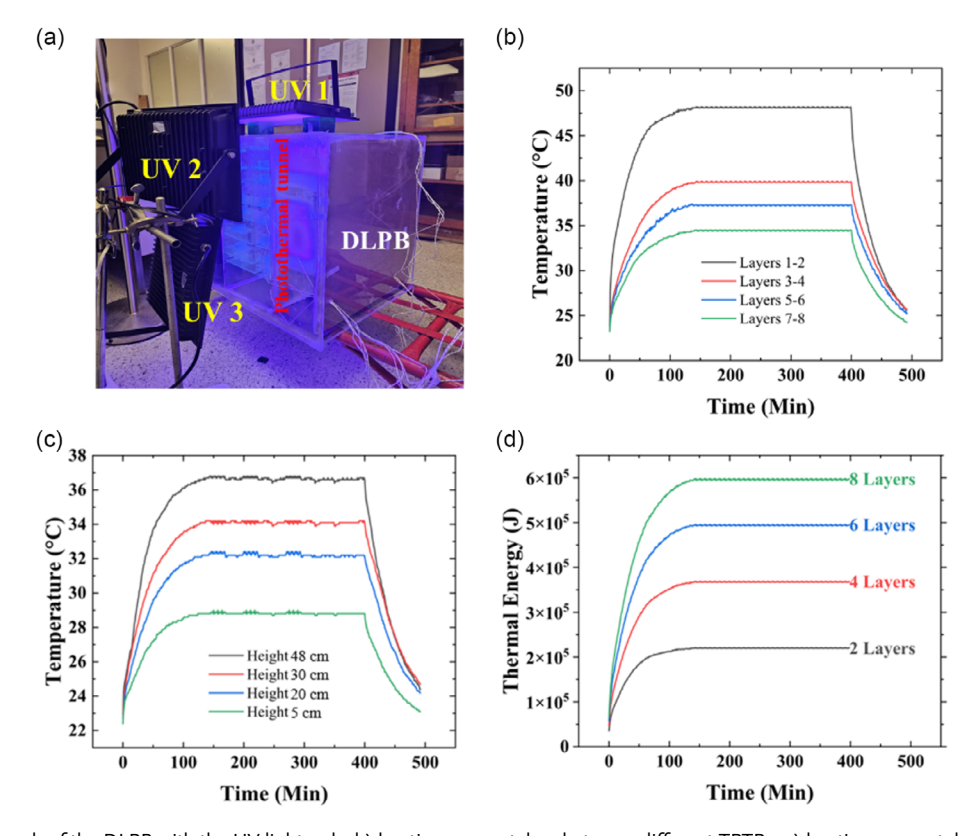


Figure 6. a) Photograph of the DLPB with the UV light only; b) heating curves taken between different TPTPs; c) heating curves taken at different heights within the DLPB, and d) thermal energy versus number of panels. Ambient temperature: 21 °C. Light power density is 15 mW cm⁻².

These observations suggest that the rate of PT heating under UV light is notably similar compared to that observed under IR light activation. Figure 6d presents the generated thermal energy corresponding to the number of TPTP utilized. The data highlight a maximum thermal energy output of up to 6.0×10^5 J with a total of eight panels, which is notably higher in comparison with the values obtained under IR light conditions (Figure 5d).

To fully utilize the absorption spectrum of Fe₃O₄@Cu_{2-x}S as shown in Figure 1a, we applied multiple UV and IR lights for more pronounced PT energy generation. As shown in Figure 7a, there are three IR lights placed in front of the DLPB. In addition, there are two UV lights in the front and one UV light on the top of DLPB (Figure 7a). However, even with multiple IR and UV lights, we have controlled the overall LPD at $15~\mathrm{mW\,cm}^{-2}$. The heating curves taken between different TPTPs are shown in Figure 7b. As can be seen in this figure, due to both UV and IR lights, the temperatures of all eight TPTP rapidly increase to the maximum of 54.8 °C. Similar behaviors are also observed for the heating curves taken at different heights within the DLPB as shown in Figure 7c. These heating curves are consistent with the diffused light sources with a much broader wavelength from UV to IR. Figure 7d shows the thermal energy generated by the number of TPTP. As can be seen in this figure, the system can generate maximum thermal energy up to 8.9×10^5 J with eight PT panels, which is much higher in comparison with those granted by UV (Figure 5d) or IR light only (Figure 6d).

The integration of light-emitting diodes (LEDs) in buildings and high rises has emerged as a pivotal strategy for achieving energy savings, economic benefits, and widespread popularity. LEDs offer unparalleled efficiency compared to traditional lighting sources, consuming significantly less energy while providing equivalent or superior illumination levels. This translates into substantial cost savings for building owners and operators through reduced electricity bills and maintenance expenses. Additionally, the long lifespan of LEDs minimizes the frequency of replacements, further contributing to economic advantages. Beyond financial considerations, LEDs have gained popularity due to their versatility in design, allowing for customizable lighting solutions tailored to the specific needs and aesthetics of different spaces. Moreover, LEDs are environmentally friendly, emitting less heat and containing no hazardous materials such as mercury, aligning with sustainability goals and regulations. As a result, the widespread adoption of LEDs in buildings and high rises not only offers tangible economic benefits but also contributes to energy conservation and environmental stewardship, making them a favored lighting choice in modern construction projects.

In addition to UV and IR lights, LEDs have been incorporated for PT energy generation. As illustrated in **Figure 8**a, four LED lights (10 W each) emitting wavelengths between 400 and 450 nm are positioned atop and in front of the DLPB. The overall LPD was controlled at 15 mW cm⁻². Heating curves captured across different TPTPs are presented in Figure 8b. Notably,

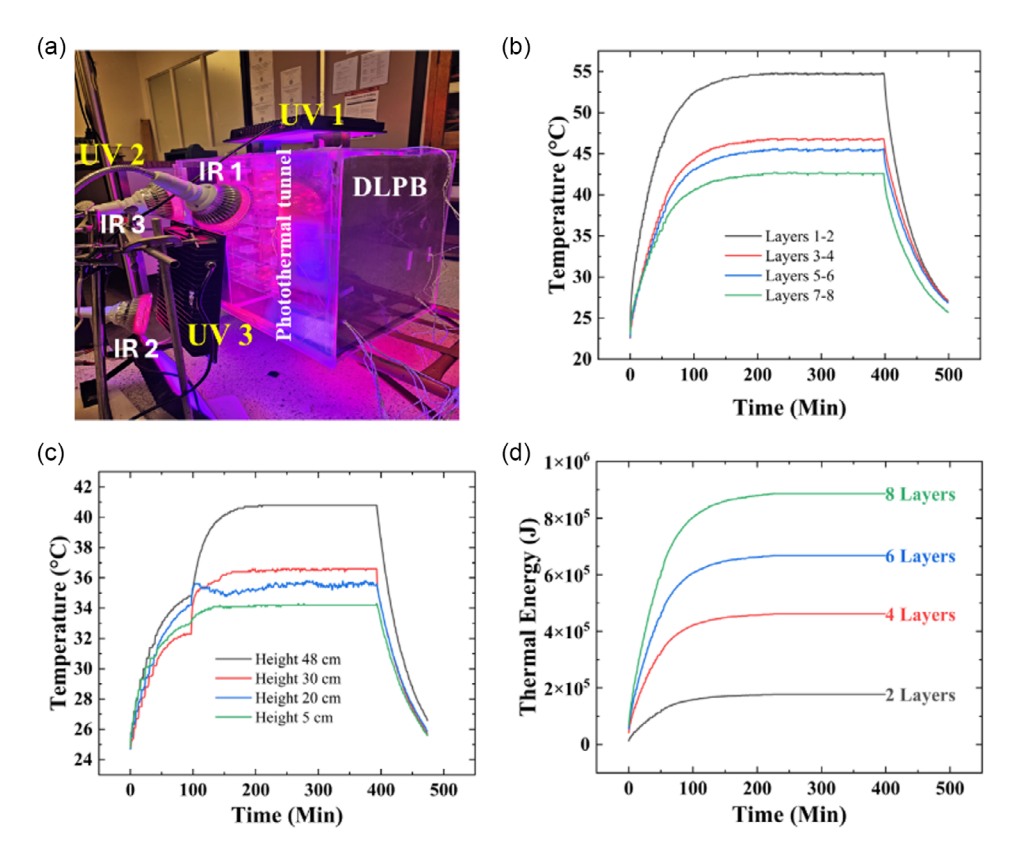


Figure 7. a) Heating curves taken between different TPTPs under both UV and IR lights; b) heating curves taken at different heights within the DLPBs under both UV and IR lights; c) thermal energy versus number of panels; and d) the heat energy generated and absorbed by each panel over time (data draw from a). Ambient temperature: 25 °C. Light power density is 15 mW cm⁻².

www.advancedsciencenews.com www.entechnol.de

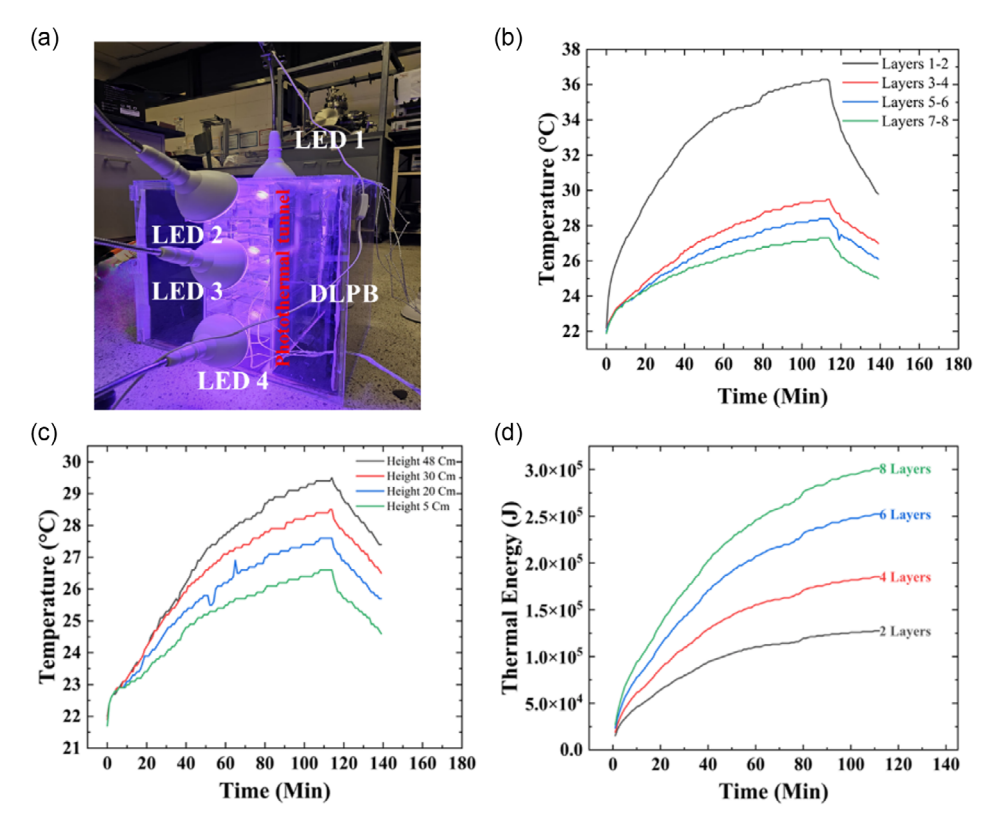


Figure 8. a) Photograph of the DLPB with the purple light (10 W each, 400–450 nm); b) heating curves taken between different TPTPs; c) heating curves taken at different heights within the DLPB, and d) thermal energy versus number of panels. Ambient temperature: 21.6 °C. Light power density is 15 mW cm^{-2} .

the introduction of LEDs results in a consistent temperature rise across all eight TPTP, with the top panel reaching 36.6 °C. The behavior observed with LEDs suggests a heightened heating power surpassing heat dissipation. Despite the considerably lower wattage of the LEDs (10 W) compared to standard UV (100 W) and IR (56 W) lights, the PT heating effect remains substantial. Analogous trends are apparent in heating curves obtained at various heights within the DLPB, as illustrated in Figure 8c. Figure 8d illustrates the thermal energy generated corresponding to the number of TPTP. Evidently, the system is capable of producing a maximum thermal energy of up to 3.35×10^5 J with eight PT panels, representing a significant increase compared to the energy generated with only two layers, indicative of notable cumulative heat generation facilitated by multiple panels.

Figure 9a depicts a photograph showcasing four LED lights (10 W each) emitting wavelengths between 585 and 620 nm, strategically positioned atop and in front of the DLPB. The heating behaviors observed in Figure 9b-d mirror those seen in Figure 8. Notably, given that LEDs emit light in the visible range, where $Fe_3O_4@Cu_{2-x}S$ absorption is minimal, as depicted in Figure 1a, the maximum temperature achieved is constrained to 28.3 °C for the top layers. Beyond the PT tunnel, the highest temperature recorded is 25.3 °C at a distance of 48 cm, with a maximum thermal energy output of 8.77×10^4 J. These experimental findings underscore the significance of spectral selectivity in plasmonic particle-mediated PT heating. Specifically, optimal photon-toheat conversion necessitates substantial UV and IR absorptions while minimizing absorption in the visible range to enable efficient AVT of the film.

The photon conversion efficiency (PCE) is calculated with the equation below:[33]

$$\eta = \frac{(C_{\rm g}m_{\rm g} + C_{\rm PTmaterial}m_{\rm PTmaterial} + C_{\rm polymer}m_{\rm polymer})\Delta T_{\rm max}}{IA\Delta t}$$

$$\approx \frac{C_{\rm g}m_{\rm g}\Delta T_{\rm max}}{IA\Delta t} \times 100\%$$
(1)

where g is the glass, is the specific heat capacity (J g^{-1} °C), m is the mass (g), ΔT_{max} is the maximum change in temperature increase in the sample (°C), I is the incident LPD (W cm $^{-2}$), A is the surface area of the sample, and Δt is the time required for a sample to reach the maximum temperature (s). $[^{33}]$

Figure 10 shows the PCE of the TPTPs obtained under different lighting conditions. With three IR lights, the PT tunnel captures low-energy photons. Due to pronounced IR absorption by Fe₃O₄@Cu_{2-x}S, the single panel attains a 19.95% PCE, and when all eight layers are combined, there is a remarkable 172% increase in net PCE compared to a single layer due to consistent light attenuation. [34,35] With three UV lights, the PT tunnel receives the high-energy photons, resulting in a PCE of a single layer to 44.43% and increases to 239.47% when adding eight panels. However, when both three UV and three IR lights are applied, the PT tunnel leads to a collective 355.43% PCE improvement across all eight layers compared to a single layer.

www.advancedsciencenews.com www.entechnol.de

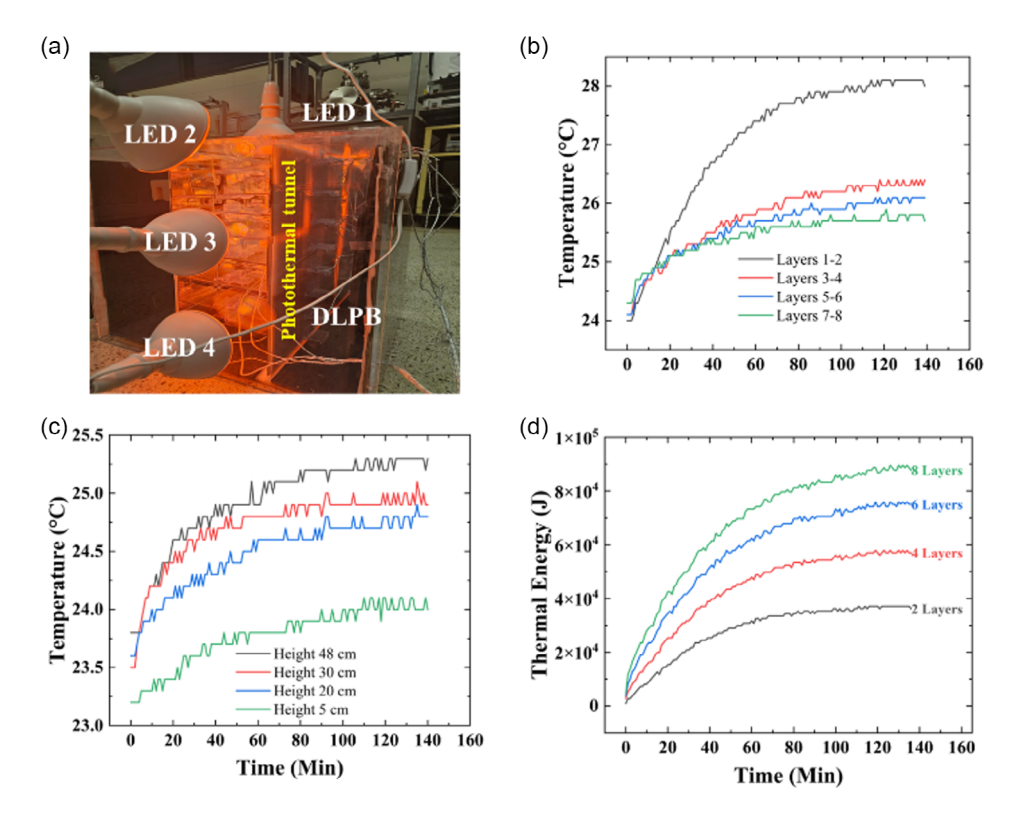


Figure 9. a) Photograph of the DLPB with the orange light (10 W each, 585–620 nm); b) heating curves taken between different TPTPs; c) heating curves taken at different heights within the DLPB; and d) thermal energy versus number of panels. Ambient temperature: 21.6 °C. Light power density is 15 mW cm⁻².

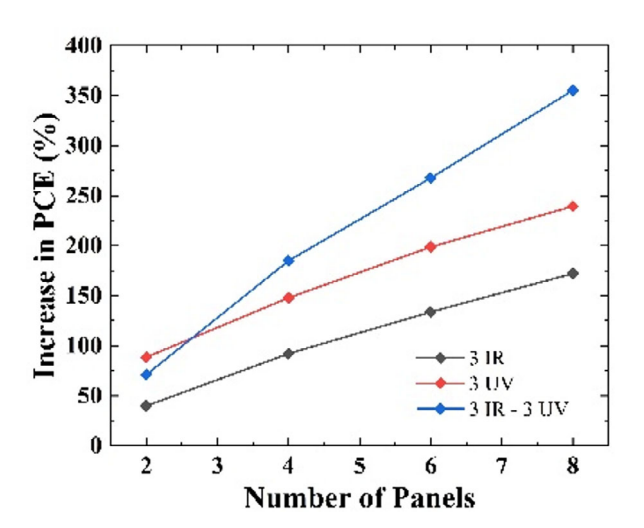


Figure 10. Increase in PCE of the PTTPs as a function of number of TPTP. The increase in PCE is calculated using Equation (1) for both covered and uncovered DLPB.

4. Discussion

As shown in Figure 5b, 6b, and 7b, upon turning on lights (i.e., IR, UV, and IR + UV), the $Fe_3O_4@Cu_{2-x}S$ thin films are photothermally activated to generate thermal energy, raising the surface temperatures as shown in the heating curves in

the first 100 min. Meanwhile, as the PT tunnel and the DLPB are not thermally insulated, heat is constantly being dissipated into the environment. This is directly reflected on the heating curves shown in Figure 5b, 6b, and 7b with different heating sources. As shown in Figure 5b, 6b, and 7b, the temperature increases are relatively rapid in the first 100 min time period, indicating efficient generation of thermal energy in the $\text{Fe}_3\text{O}_4\text{@Cu}_{2-x}\text{S}$ thin films. However, once the heat loss balances the thermal energy generated by the $\text{Fe}_3\text{O}_4\text{@Cu}_{2-x}\text{S}$ thin films, the heating curves exhibit plateaus until the lights are turned off at 400 min as shown in Figure 5b, 6b, and 7b.

The heat dynamics observed in the TPTPs are pivotal to the overall performance of the DLPB. As depicted in Figure 9, the TPTPs with their relatively low specific heat capacity (78 J kg⁻¹ K) demonstrate rapid heat dissipation characteristics. **Figure 11** provides a comprehensive illustration of the dynamic interplay between heat generation and dissipation within the TPTP. Notably, the initial rapid temperature rises observed in the heating curves (Figure 5b, 6b, and 7b) are mirrored in the spikes depicted in Figure 11 for all different lighting conditions. These spikes highlight the swift response of the TPTP to the onset of light exposure, showcasing their ability to quickly generate heat. Similarly, the appearance of spikes upon the cessation of light exposure indicates the panels' rapid cooling behavior.

Furthermore, the heating curves from Figure 5b, 6b, and 7b reveal intriguing differences in heating rates under varying lighting conditions. When exposed to three IR lights

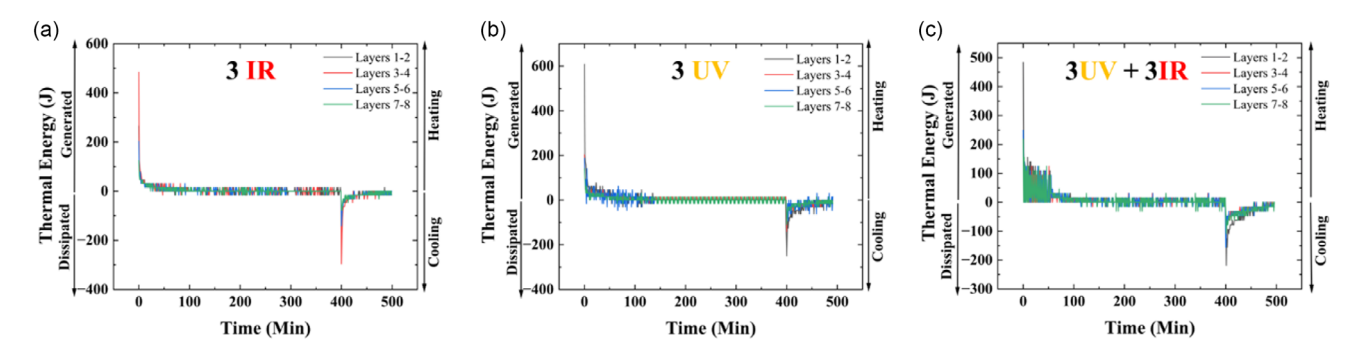


Figure 11. The thermal energy generated and dissipated by the PT panels over time as indicated based on data draw from a) Figure 5b, b) Figure 6b, and c) Figure 7b.

(Figure 5b), the initial heating rates are measured at 0.2 °C min⁻¹. However, this heating rate increases 0.41 °C min⁻¹ when the TPTP are subjected to three UV lights (Figure 6b). The heating rate further increases to 0.51 °C min⁻¹ under three UV and three IR lights. This observation points toward the synergistic effect of combined IR and UV light exposure on the heat generation capabilities of the TPTP. Overall, the collective data presented in Figure 5b, 6b, 7b, and 11 elucidate a balanced equilibrium between the thermal energy generated by the TPTP and the subsequent heat loss into the surrounding space. This balance, reflected in the heating curve plateaus, indicates the efficiency of the TPTP in effectively dissipating generated thermal energy. It is this precise control overheat dynamics that contributes significantly to the optimal performance and energy efficiency of the DLPB system which is a basic model for the PT radiator as depicted in Figure 2.

The heating curves shown in Figure 5-9 are directly associated with the PT effects of the Fe₃O₄ @Cu_{2-x}S nanoparticles. As shown in Figure 1a, there are distinct optical behaviors between the Fe₃O₄ and Fe₃O₄ @Cu_{2-x}S nanoparticles resulting from their unique electronic structures and the core-shell architecture. [19,27,29-31] Fe₃O₄, being a mixed-valence iron oxide, exhibits semiconducting properties with a narrow bandgap andnotable magnetic characteristics, influencing its optical response in the UV region. [19,27] In contrast, the Fe₃O₄ @Cu_{2-x}S nanoparticles benefit from the $Cu_{2-x}S$ shell, which introduces LSPR in the IR region. ^[19,27,29–31] The LSPR in $Cu_{2-x}S$ nanocrystals is highly tunable based on size, shape, and stoichiometry, allowing precise control over their optical properties. [19,27,29-31] This tunability is critical for optimizing IR absorption and facilitates several energy conversion mechanisms, such as efficient PT conversion and hot electron generation, useful for photocatalytic reactions.

By manipulating the size and morphology of $Cu_{2-x}S$ nanoparticles, their IR absorption capabilities can be well enhanced. [19,27,29–31] Smaller nanocrystals shift LSPR to shorter wavelengths, while larger ones move it to longer wavelengths. [19,27,29–31] The shape of the nanocrystals, such as rod-like or spherical, also affects the LSPR, with anisotropic shapes offering multiple plasmon modes. Additionally, the copper deficiency in $Cu_{2-x}S$ (represented by x) alters the carrier density and consequently the LSPR frequency. [19,27,29–31]

Core–shell structureslike Fe_3O_4 @ $Cu_{2-x}S$ can further enhance optical properties through optoelectronic coupling between the core and shell. This ability to fine-tune the nanoparticles' properties makes them ideal for applications in PT therapy, catalysis, solar energy harvesting, and other technologies requiring controlled IR absorption and energy conversion.

As outlined in the experimental procedures, the IR and UV lamps emit light within specific wavelength ranges, with the IR lamp covering the NIR spectrum of 660-850 nm and the UV lamp emitting wavelengths of 380-420 nm, respectively. While the UV light aligns well with the absorption spectrum of $Fe_3O_4@Cu_{2-x}S$ in this region, the IR light is limited to the NIR wavelength range, which does not coincide with the absorption peak of Fe₃O₄@Cu_{2-x}S at 1150 nm. This limited frequency range of the IR lights is responsible for less effective PT heating (Figure 5) in comparison with the UV lights (Figure 6). Therefore, it is anticipated that a much stronger PT effect could be achieved by utilizing IR light with emission wavelengths closer to the absorption peak of Fe₃O₄@Cu_{2-x}S. This strategic alignment of light source wavelengths with the absorption characteristics of Fe₃O₄@Cu_{2-x}S holds the potential to significantly enhance the PT efficiency of the system.

The utilization of LED lights for PT heating, as demonstrated in the study, presents an intriguing avenue for sustainable energy generation in indoor environments. The incorporation of LEDs emitting wavelengths within the visible spectrum, despite lower absorption rates by Fe₃O₄@Cu_{2-x}S nanoparticles compared to UV and IR wavelengths, still showcases significant potential for heating applications. This underscores the resilience of LED-generated PT effects, even within the visible spectrum, albeit to a lesser extent in the initial light irradiation time period. These findings highlight the importance of spectral selectivity in plasmonic particle-mediated PT heating, emphasizing the need for tailored absorption properties to optimize energy conversion efficiency. Moving forward, further exploration into optimizing LED configurations and spectral characteristics could unlock greater potential for harnessing LED-generated PT heating in building environments, offering a promising avenue for enhancing energy efficiency and sustainability. As shown in this study, the swift response, efficient heat dissipation, and synergistic heat generation capabilities of the transparent PT panels play a pivotal role in the overall functionality of the DLPB. These findings further indicate the potential of TPTP as a promising



technology for sustainable energy applications, offering a glimpse into the dynamic interplay of heat dynamics within the DLPB system.

5. Summary

This study demonstrates the potential of generating heat using diffused light through the PT effect of plasmonic Fe₃O₄@Cu_{2-x}S nanoparticles. Transparent Fe₃O₄@Cu_{2-x}S thin films achieved significant results, raising temperatures within the DLPB by up to 54.8 °C. By exploiting the UV and IR absorption properties of Fe₃O₄@Cu_{2-x}S, we utilized PT heating via LSPR. Our research aims to improve energy efficiency in buildings by developing a PT radiator capable of utilizing diffused light for heat generation. This technology targets energy-neutral buildings, particularly focusing on enhanced efficiency during nighttime and rainy days. By incorporating plasmonic Fe₃O₄@Cu_{2-x}S nanoparticles into transparent thin films, we provide a sustainable solution for maintaining comfortable indoor temperatures without heavy reliance on traditional energy sources. The innovative system uses UV and IR lights to activate transparent PT thin films, ensuring optimal energy capture even in low-light conditions such as cloudy days or nighttime hours. Within the DLPB, the system effectively raises temperatures above 50 °C using diffused UV and IR lights, showcasing its potential for sustainable heat generation in indoor environments. Leveraging the robust UV and IR absorptions of Fe₃O₄@Cu_{2-x}S nanoparticles through LSPR, this novel PT radiator sets the stage for a more energyefficient future in building heating and comfort control.

The incorporation of LEDs into the PT energy generation system offers several advantages, including energy efficiency, utilizing diffused indoor lights for prolonged period of time, and potential cost savings. LEDs are renowned for their energy efficiency, consuming significantly less power compared to traditional lighting sources while still providing ample illumination. Additionally, LEDs allow for precise control over the emitted light wavelengths, enabling tailored spectral characteristics optimized for PT heating applications. This flexibility in wavelength selection ensures efficient energy conversion by matching the absorption spectra of plasmonic nanoparticles, such as Fe₃O₄@Cu_{2-x}S, thereby maximizing PT conversion efficiency. Moreover, the use of LEDs can lead to substantial cost savings over the long term due to their extended lifespan and reduced energy consumption, making them an economically viable option for sustainable energy generation in building environments.

Acknowledgements

The authors acknowledge the financial support from National Science Foundation CMMI-1953009 and the Michelman Green, Clean and Sustainable Technology Research Innovation Program (F103484).

Conflict of Interest

The authors declare no conflict of interest.

Data Availability Statement

The data that support the findings of this study are available on request from the corresponding author. The data are not publicly available due to privacy or ethical restrictions.

Keywords

diffused light, energy-neutral buildings, photothermal utility heating, plasmonic nanoparticles, transparent multipanels

Received: April 6, 2024 Revised: May 29, 2024 Published online:

- [1] U.S. Energy Information Administration (EIA), Consumption and Efficiency, https://www.eia.gov/consumption/ (accessed: October 2020)
- [2] F. Perera, Int. J. Environ. Res. 2018, 15, 16.
- [3] M. S. Dresselhaus, I. L. Thomas, Nature 2001, 414, 332.
- [4] M. Graetzel, Inorg. Chem. 2005, 44, 6842.
- [5] R. H. Bube, *Photovoltaic Materials*, Imperial College Press, London, UK 1998.
- [6] V. Weitbrecht, D. Lehmann, A. Richter, Sol. Energy 2002, 73, 433.
- [7] R. Fu, D. Feldman, R. Margolis, M. Woodhouse, K. Ardani, Solar Photovoltaic System Cost Benchmark: Q1, U.S. Department of Energy Office of Scientific and Technical Information, Washington, D.C. 2017, https://doi.org/10.2172/1395932.
- [8] I. Nath, J. Int. Relat. 2010, 11, 6.
- [9] P. Irace, H. Brandon, Mechanical Engineering and Materials Science Independent Study, Washington University in St. Louis, Vol. 50 2017, https://openscholarship.wustl.edu/mems500/50.
- [10] A. Jamar, Z. A. A. Majid, W. H. Azmi, M. Norhafana, A. A. Razak, Int. Commun. Heat Mass Transfer 2016, 76, 178. ISSN 0735-1933.
- [11] J. Moral-Carcedo, J. Pérez-García, Energy Effic. 2021, 14, 68.
- [12] A. M. Al-Ghaili, H. Kasim, N. M. Al-Hada, M. Othman, M. A. Saleh, IEEE Access 2020, 8, 76108.
- [13] N. Gentile, Energy Build. 2022, 263, 112022. ISSN 0378-7788.
- [14] M. Seminara, M. Meucci, F. Tarani, C. Riminesi, J. Catani, *Photonics Res.* 2021, 9, 548.
- [15] E. Hutter, J. H. Fendler, Adv. Mater. 2004, 16, 1685.
- [16] J. Zhao, X. Zhang, C. R. Yonzon, A. J. Haes, R. P. Van Duyne, Nanomedicine 2006, 1, 219.
- [17] X. Huang, P. K. Jain, I. H. El-Sayed, M. A. El-Sayed, Lasers Med. Sci. 2008, 23, 217.
- [18] Y. Zhao, M. E. Sadat, A. Dunn, H. Xu, C.-H. Chen, W. Nakasuga, R. C. Ewing, D. Shi, Sol. Energy Mater. Sol. Cells 2017, 161, 247.
- [19] M. Lyu, J. Lin, D. Shi, Energy Technol. 2021, 9, 2100590.
- [20] M. Lyu, J. Lin, J. Krupczak, D. Shi, Adv. Sustainable Syst. 2021, 5, 2100006.
- [21] J. Lin, J. Krupczak, D. Shi, MRS Commun. 2022, 12, 1225.
- [22] J. Lin, Y. Wang, M. Lyu, D. Shi, Sol. Energy Mater. Sol. Cells 2022, 243, 15.
- [23] M. Lyu, J. Lin, J. Krupczak, D. Shi, MRS Commun. 2020, 10, 439.
- [24] M. E. Sadat, M. K. Baghbador, A. W. Dunn, H. P. Wagner, R. C. Ewing, J. Zhang, H. Xu, G. M. Pauletti, D. B. Mast, D. Shi, *Appl. Phys. Lett.* 2014, 105, 091903.
- [25] A. W. Dunn, Y. Zhang, D. Mast, G. M. Pauletti, H. Xu, J. Zhang, R. C. Ewing, D. Shi, *Mater. Sci. Eng.*, C 2016, 69, 12.
- [26] D. Shi, M. E. Sadat, A. W. Dunn, D. B. Mast, Nanoscale 2015, 7, 8209.

www.advancedsciencenews.com www.entechnol.de

- [27] J. Lin, Y. Zhao, D. Shi, MRS Commun. 2020, 10, 155.
- [28] J. Lin, J. Krupczak, D. Shi, MRS Commun. 2022, 12, 1225.
- [29] A. J. Haes, S. Zou, G. C. Schatz, R. P. Van Duyne, J. Phys. Chem. B 2004, 108, 109.
- [30] Q. Tian, J. Hu, Y. Zhu, R. Zou, Z. Chen, S. Yang, R. Li, Q. Su, Y. Han, X. Liu, J. Am. Chem. Soc. 2013, 135, 8571. Epub 2013 May 30. PMID: 23687972
- [31] Q. Tian, J. Hu, Y. Zhu, R. Zou, Z. Chen, S. Yang, R. Li, Q. Su, Y. Han, X. Liu, J. Am. Chem. Soc. 2013, 135, 8571.
- [32] A. Katepalli, Y. Wang, J. Lin, A. Harfmann, M. Bonmarin, J. Krupczak, D. Shi, Sol. Energy 2024, 271, 112444.
- [33] J. Lin, D. Shi, Appl. Phys. Rev. 2021, 8, 011302.
- [34] J. Lin, M. Lyu, D. Shi, Energies 2023, 16, 3173.
- [35] A. Katepalli, Y. Wang, D. Shi, Sol. Energy 2023, 264, 112047.